

## A Pacific Moisture Conveyor Belt and Its Relationship to a Significant Precipitation Event in the Semiarid Southwestern United States

PETER KNIPPERTZ AND JONATHAN E. MARTIN

*Department of Atmospheric and Oceanic Sciences, University of Wisconsin—Madison, Madison, Wisconsin*

(Manuscript received 23 September 2005, in final form 12 April 2006)

### ABSTRACT

In this study the term moisture conveyor belt (MCB) is defined as an elongated band of enhanced poleward water vapor fluxes (WVFs) above the PBL that is rooted in the Tropics. This new terminology is illustrated through an exemplary detailed case study of an MCB over the northeastern Pacific during 9–13 November 2003 that provides the moisture for a significant precipitation event in the dry southwestern United States. The analysis of the involved moisture transports and dynamics comprises both Eulerian and Lagrangian approaches, and is based upon output from a simulation with the University of Wisconsin–Nonhydrostatic Modeling System, as well as analysis data, surface observations, and satellite images.

The formation of the MCB is related to a quasi-stationary upper-level cutoff low (COL) resulting from a wave-breaking event over the North Pacific. A pronounced upper-tropospheric baroclinic zone and a strong, inertially unstable subtropical jet (STJ) are found to the east of the COL, where at later stages an elongated tropical cloud plume developed in association with a marked flare-up of ITCZ convection. Part of the extratropical air that subsides to the west of the COL becomes involved in this convection; another part feeds the so-called dry slot at the base of the COL. The actual MCB consists of midlevel trajectories that curve anticyclonically away from the moist tropical easterlies and cause a northeastward-directed WVF maximum at around 700 hPa over the subtropical northeast Pacific and a marked humidity gradient toward the subsided extratropical air. At late stages, frontogenetic circulations lead to WVF convergence involving air from the midlevel subtropical troposphere. At the surface, cyclogenesis and thermal contrasts are weak, and northeasterly trade winds prevail, which clearly distinguishes this MCB from a classical extratropical warm conveyor belt. Other important differences are the high elevation of the WVF maximum, as well as the quasi-horizontal track and origin above the PBL of most moist trajectories. Three precipitation regions with different influence factors can be distinguished. 1) Close to the COL center, moist tropical air is overrun by the dry slot, resulting in convective instability and extreme hail in the Los Angeles, California, area. 2) To the north and east, quasigeostrophic forcing and midlevel warm frontogenesis generate ascent, where the northern branch of the MCB circulates around the COL. 3) Along the anticyclonic shear side of the STJ, convection forms within potentially unstable MCB air benefiting from the inertial instability at the outflow level. It is suggested that this set of circumstances is quite similar to those that conspire to produce heavy precipitation events in subtropical West Africa.

### 1. Introduction

A number of studies have related extraordinary cool season precipitation events in western North America to bands of enhanced moisture transport from low latitudes in connection with landfalling extratropical cyclones from the Pacific Ocean (e.g., Higgins et al. 2000; Cavazos and Rivas 2004; Ralph et al. 2004; Bao et al.

2006). The fairly frequent bands connecting Hawaii with the Pacific Northwest region are widely known as the “pineapple express.”

Methodically, the approaches employed to describe and analyze transports of water vapor (WV) differ with respect to the usage of Eulerian, Lagrangian, or pseudo-Lagrangian perspectives. Eulerian approaches usually involve a consideration of water vapor fluxes (WVFs)  $q \cdot \mathbf{v}$ , with  $q$  and  $\mathbf{v}$  being, respectively, specific humidity and the horizontal vector wind at a given pressure level. Often WVFs are integrated over the depths of the atmosphere to get vertically integrated water vapor fluxes (IWVFs). Given the almost exponential de-

---

*Corresponding author address:* Dr. Peter Knippertz, Institut für Physik der Atmosphäre, Johannes Gutenberg-Universität Mainz, D-55099 Mainz, Germany.  
E-mail: knippertz@uni-mainz.de

crease of specific humidity with decreasing pressure, IWVFs are largely determined by the layer between the surface and 500 hPa, where about 90% of the total water vapor is concentrated. Zhu and Newell (1994) coined the term “atmospheric rivers” for narrow filaments of high IWVF. The same authors find that more than 90% of the total meridional IWVF at midlatitudes in a model is accomplished by, on average, four to five such atmospheric rivers covering less than 10% of the hemispheric circumference (Zhu and Newell 1998). Moisture transports in connection with extratropical cyclones often appear as narrow bands of high vertically integrated water vapor (IWV) on Special Sensor Microwave Imager (SSM/I) satellite images, even without explicit flux calculations (Ralph et al. 2004; Bao et al. 2006).

A widely used pseudo-Lagrangian approach for describing moisture transports in connection with extratropical cyclones is the “warm conveyor belt” (WCB) concept, which is based on (classically isentropic or moist-isentropic) trajectories relative to the movement of the center of the cyclone (Carlson 1980; Browning 1990). The WCB is located ahead of the surface cold front, where strong horizontal temperature gradients cause the formation of a front-parallel low-level jet through the thermal wind relationship. Typically the warm and moist WCB air originates in the planetary boundary layer (PBL), often over a warm ocean surface, and then ascends and contributes to the formation of frontal cloud and precipitation bands.

From an Eulerian perspective WCBs are characterized by a front-parallel WVF maximum, usually at around 900 hPa (e.g., Fig. 9a in Ralph et al. 2004). Given the moderate change in wind direction with height at lower levels within a typical warm sector, WCBs are also prominent features in IWVF fields. Fast-moving cyclones might produce a nonnegligible WVF (or IWVF) component in the across-frontal direction, which is absent in the classical storm-relative analysis. In addition, WCBs appear as elongated bands in satellite-derived IWV fields that tend to get narrower and more intense in the vicinity of extratropical cyclones (Ralph et al. 2004; Bao et al. 2006). This narrowing points to horizontal WVF convergence associated with frontogenetic circulations. From a Lagrangian perspective, classical WCBs can be identified as featuring the passage of trajectories with similar characteristics over a time period of several days (Wernli 1997). Among these salient characteristics are an origin in the PBL and a subsequent rapid upward, poleward, and eastward track.

Several problems arise when the originally midlatitude WCB concept is applied to moisture transports

from low latitudes. In the subtropics extratropical disturbances often take the form of slowly moving or quasi-stationary cutoff lows (COLs) or troughs. Despite a distinct positive potential vorticity (PV) anomaly at upper levels, the associated cyclonic circulation is often not troposphere-deep because of the small Coriolis parameter and the generally high static stability in the subtropics (Hoskins et al. 1985, section 3). This has far-reaching impacts on the characteristics of the associated WVFs.

- The lack of a significant low-level manifestation of the circulation implies that poleward moisture transports will occur at midlevels rather than in the PBL. Given that the extratropical disturbance affects sufficiently low latitudes, tropical air masses can be incorporated into the circulation. Because of warm temperatures and deep convective mixing in the Tropics, specific humidity is still relatively high at midlevels and can therefore fuel significant poleward moisture transports above the PBL in contrast to typical conditions at midlatitudes.
- The midlevel circulation is not affected by frictional convergence, which can be a dominating factor in low-level frontogenesis, even over the ocean (e.g., Bond and Fleagle 1985). This hinders the formation of sharp frontal zones and associated low-level jets, so that we expect midlevel moisture transports in connection with a subtropical disturbance to be relatively slow.
- Weak midlevel fronts have weak secondary frontal circulations and therefore feeble ascending motions on the warm side of the front. Moisture transports along such a front will occur quasi-horizontally and possibly without a significant cloud feature.
- The subtropical free troposphere is affected by subsidence associated with both the poleward branch of the Hadley cell and extratropical waves and is therefore a generally dry environment. Consequently, bands of moisture transport from the much wetter Tropics will be prominent features in IWV fields and, if the circulation is sufficiently strong, also in WVF or even IWVF fields. However, without distinct low-level temperature contrasts, the moisture transport will not be in concert with significant transports of heat.

Bao et al. (2006) observed a relation between trajectories from the Tropics and high-IWV bands over the eastern North Pacific and suggested terming them “moisture conveyor belts” (MCBs). The study, however, does not provide a detailed definition of this term and because it is based on IWV estimates only, the vertical structures of the moisture transports are not

examined. We regard this new terminology as adequate for the phenomenon described above, because it retains a certain analogy to WCBs, but stresses the predominant transport of latent rather than sensible heat. We will now try to give a definition based on the fundamental considerations described in the previous paragraph. For the remainder of the paper the term MCB shall be used for *elongated bands of enhanced poleward WVFs above the PBL that are rooted in the Tropics*. Because moisture fluxes in the PBL might occur in a different direction than within the MCB, equally distinct local maxima of IWVFs are not required for this definition. Consequently, there might be MCBs that would not be termed atmospheric rivers. We do, however, expect MCBs to leave a clear sign in IWV fields in the subtropics.

In contrast to the classical WCB, the MCB definition given above is based on Eulerian quantities. Given the relatively slow moisture transports in the subtropical midtroposphere, we expect that a quasi-stationary upper trough or COL is needed to allow for the formation of an MCB. Therefore, differences between Lagrangian, pseudo-Lagrangian, and Eulerian approaches will, in most cases, be much smaller than those for the fast-moving cyclones at midlatitudes. Other significant differences from WCBs are that the moisture transports do not necessarily originate in the PBL, but occur mostly quasi-horizontally at midlevels, and are not necessarily accompanied by significant sensible heat transports nor a frontal cloud band. We also expect differences with respect to precipitation. While WCB are usually associated with widespread frontal rain (or snow), MCB precipitation will depend on several additional factors. If the ascent generated by the extratropical disturbance related to the MCB is sufficiently strong, frontal-like precipitation can occur, too. If not, the associated moisture transports could still lead to a destabilization of the atmosphere that, together with other factors (mountains or warming of land surfaces, etc.), can lead to convective instability. Of course in some cases there will be a transition from an MCB to a WCB in the vicinity of the extratropical disturbance, so that a clear distinction between the two concepts will not be possible.

MCBs, according to our definition, have to be clearly demarcated from “tropical plumes” (TPs). This term refers to elongated, poleward- and eastward-oriented, continuous bands of upper- and midlevel clouds anchored in the Tropics, which are frequently observed over the central and eastern North Pacific (McGuirk et al. 1987; Kuhnelt 1989). Typically, TPs form on the downwind side of an upper-level subtropical trough and are accompanied by a subtropical jet (STJ) streak (e.g.,

McGuirk et al. 1988; Knippertz 2005). In some cases the strong anticyclonic shear at the equatorward side of the STJ leads to inertial instability, which supports the intensification of convection by facilitating the ventilation of upper-level outflow (Blanchard et al. 1998; Knippertz and Martin 2005). Definitions of TPs are based on IR satellite imagery (McGuirk et al. 1987; Iskenderian 1995) and therefore do not imply information on WVFs. This is not to say that TPs and MCBs (or even WCBs) cannot occur simultaneously, as various studies document low-level frontal bands along the northwestern edge of TPs.

There are a number of studies in the literature that find indications for the occurrence of MCBs. For instance, Bao et al. (2006) observe that IWV maxima over the eastern North Pacific are not always aligned with the surface pressure field at low latitudes as they are in the vicinity of an extratropical cyclone. This suggests significant contributions from midlevel moisture transports. In a detailed case study of an intense IWV band, Ralph et al. (2004) find a fairly complicated structure at low latitudes with two frontal zones and a very different distribution of moisture in the lower and middle troposphere. Their composite analysis reveals a strong latitudinal dependence of the IWV band characteristics. Kiladis (1998) relates enhanced tropical convection/TP formation over the central North Pacific with Rossby wave trains from the midlatitudes and finds baroclinic wave characteristics in the extratropics, but more complicated structures at low latitudes. A climatological study based on the trajectory analysis by Wernli (1997) shows very few WCBs over the subtropical eastern Pacific (Eckhardt et al. 2004), suggesting a relation between the fairly frequent enhanced IWV bands and MCBs.

The present paper investigates the evolution of an MCB over the northeastern Pacific Ocean during 9–13 November 2003. The event was associated with an upper-level COL off the coast of California and was accompanied by significant precipitation in the arid southwestern United States, as well as a locally intense hailstorm in the Los Angeles, California, area. At late stages a TP develops above the MCB. The aim of this study is to illustrate the characteristics and physical mechanisms involved in the moisture transports and to justify the usage of the MCB term. The investigations are based on a simulation of the event using the University of Wisconsin-Nonhydrostatic Modeling System (UW-NMS) with 75-km resolution. This does not allow for a detailed analysis of the finescale structure of precipitation, which is clearly beyond the scope of this paper, but the 2-h temporal resolution of the model out-

put allows for the calculation of accurate trajectories in order to analyze the contribution of single air parcels to the MCB moisture transports and to show modifications along the trajectory paths.

The remainder of the paper is organized as follows. Section 2 provides basic information on data, computational methods, and the UW-NMS. Section 3 contains a description of the precipitation event based on both observations and model data, and section 4 gives an overview of the synoptic evolution including the large-scale upstream development that produced the COL. In section 5 we contemplate the region of subsidence and dryness to the north of the MCB-TP and analyze its interactions with tropical convection and the precipitation over North America. This point has received little attention in other studies of low-latitude MCBs. The formation of the MCB itself and the generation of precipitation is investigated in section 6. We assume a Lagrangian and an Eulerian perspective by using both trajectories, and vertical and horizontal distributions of WVF and WVF convergence. The paper concludes with a summary and discussion in section 7.

## 2. Data

The current study is based on a numerical simulation of the November 2003 event performed using the UW-NMS (Tripoli 1992) on a single  $160 \times 97$  point grid with 75-km grid spacing and 40 vertical levels up to 22.6 km. The model domain spans from  $15^{\circ}\text{S}$ ,  $174^{\circ}\text{W}$  to  $50^{\circ}\text{N}$ ,  $66^{\circ}\text{W}$ . The simulation was initialized at 0000 UTC 7 November 2003 and was then run until 1800 UTC 15 November. For both initialization and a four times daily (0000, 0600, 1200, and 1800 UTC) model update at the boundaries, the Global Forecast System (GFS) analyses at  $1^{\circ} \times 1^{\circ}$  horizontal resolution on standard pressure levels were used. In this way a physically consistent “interpolation” of the analyses was produced. More details on the model configuration can be found in Mecikalski and Tripoli (2003).

The visualization software VIS5D (Hibbard et al. 1996) was used for trajectory computation from the 2-hourly model output and for a three-dimensional data display to aid interpretation. For comparison, extensive ensembles of trajectories were calculated using the Lagranto algorithm by Wernli and Davies (1997) based on 6-hourly European Centre for Medium-Range Weather Forecasts (ECMWF) analysis at  $0.5^{\circ} \times 0.5^{\circ}$  horizontal resolution on model levels. Interpolation to isentropic levels and the computation and display of streamlines and various other meteorological parameters were done with routines from the General Meteorological Analysis Package. The Space Science and

Engineering Center of the University of Wisconsin—Madison provided IR and water vapor (WV) images from *Geostationary Operational Environmental Satellite-10 (GOES-10)*. ECMWF Tropical Ocean and Global Atmosphere (TOGA) operational analyses at  $2.5^{\circ} \times 2.5^{\circ}$  horizontal resolution (Trenberth 1992) were used for comparison of the large-scale features. The employed precipitation data are described in section 3.

## 3. Precipitation

Figure 1 shows 6-hourly accumulated precipitation and 500-hPa geopotential heights from the 3-hourly National Centers for Environmental Prediction North American Regional Reanalysis (NARR) at 32-km horizontal resolution (Mesinger et al. 2006). NARR comprises an extensive analysis of observed precipitation information from gauges, satellites, and radars disaggregated to 1 h, which is then assimilated into the analysis model by converting precipitation into latent heating. Here, we use this data as a best estimate of the spatial distribution of rainfall that also provides a distinction between large- and subgrid-scale precipitation.

At 0600 UTC 12 November, a COL with a central height minimum of 5621 geopotential meters (gpm hereafter) is located over the Pacific Ocean to the west of San Diego, California (Fig. 1a). Over the following 6 h, light precipitation is observed underneath the diffluent flow well east of the COL center, mainly over southern California and the southern half of Arizona (Fig. 1a). Between 1200 and 1800 UTC 12 November, the COL deepens to 5585 gpm and slowly approaches the southern California coast (Figs. 1b,c). During this period, precipitation accumulates to more than 20 mm over the mountains in southern California and toward Death Valley, affecting parts of the Mojave and Sonora Deserts (Fig. 1b). Heavy rainfalls are also analyzed over central Arizona. Between 1800 UTC 12 November and 0000 UTC 13 November, the rainfall over California spreads out into southern Nevada, while the precipitation region over Arizona intensifies and stretches into northwestern New Mexico (Fig. 1c). Overall the portion of subgrid-scale convection (thin black lines in Fig. 1) is small except for localized events in southernmost California and parts of Arizona (Figs. 1a–c).

At 0000 UTC 13 November, the COL center reaches the coast just to the northwest of Los Angeles with little change in intensity (Fig. 1d). The region of moderate, partly subgrid-scale precipitation close to the COL center contains the localized hailstorm in south-central Los Angeles mentioned in the introduction. According to the National Weather Service Los Angeles Annual Weather Review, the storm that “will probably never

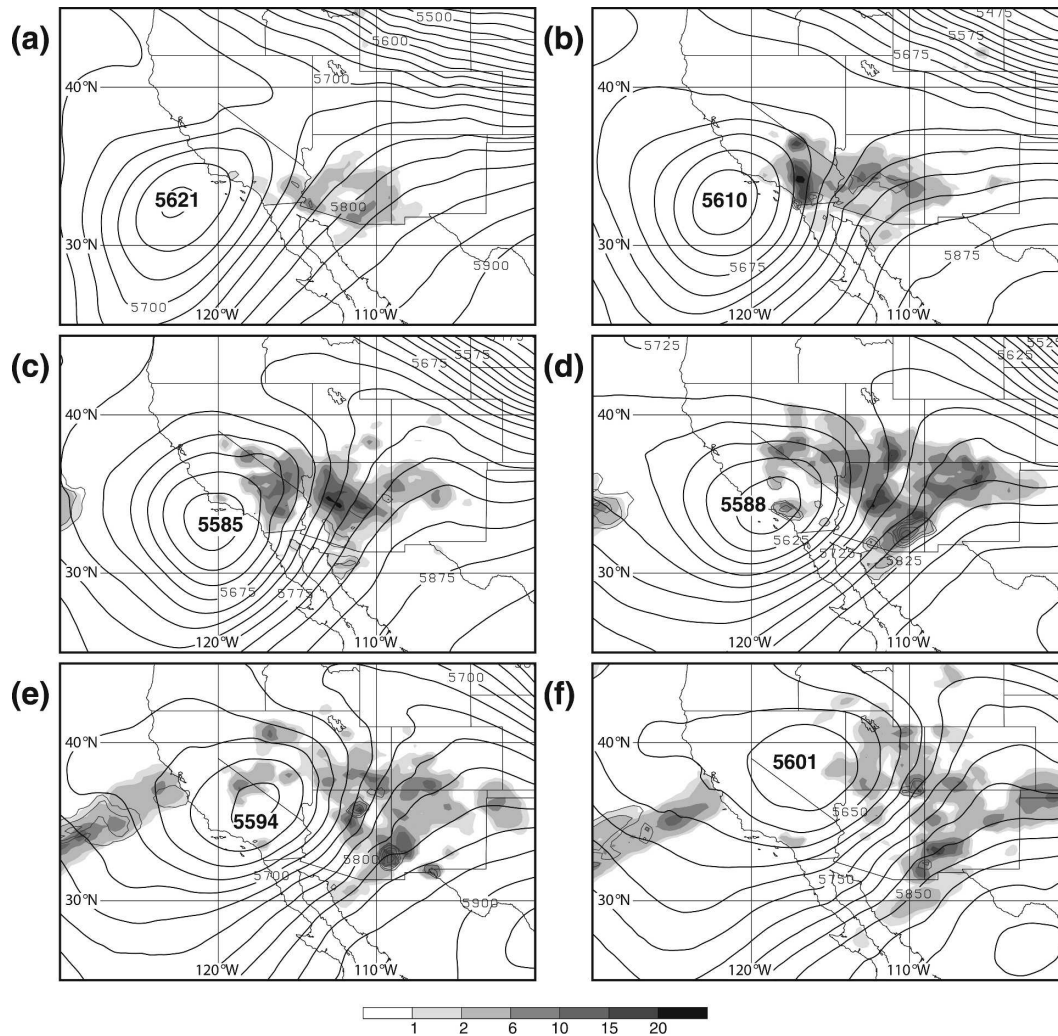


FIG. 1. The 6-h accumulated total (shading in mm) and convective precipitation (thin isopleths contoured with the same intervals as the total precipitation) from the NARR starting at (a) 0600 UTC 12 Nov, (b) 1200 UTC 12 Nov, (c) 1800 UTC 12 Nov, (d) 0000 UTC 13 Nov, (e) 0600 UTC 13 Nov, and (f) 1200 UTC 13 Nov 2003. The thick isopleths (contoured every 25 gpm) depict the 500-hPa geopotential height at the beginning of the respective period. The geopotential height minima are also indicated.

be forgotten” (National Weather Service Los Angeles 2004, personal communication) dumped copious amounts of rain and hail (136 mm in 3 h at 96th Street and Central Ave.), while just a few miles to the north, downtown Los Angeles received a mere 16 mm. According to the *New York Times* (Broder and Dixon 2003), the accompanying lightning strikes took down power pylons and cut power to about 115 000 customers. Wind gusts forced the temporary closure of Los Angeles International Airport, and firefighters rescued more than 100 people from cars and flooded streets.

Away from the COL center a fairly large region of moderate-to-heavy precipitation covers Arizona, northern New Mexico, southwestern Colorado, and southern Utah, while lighter rainfall wraps around the

COL center across southern Nevada into central California (Fig. 1d). The easternmost rainfalls are already located under the ridge downstream of the COL center. Contributions from subgrid-scale convection are confined to the southernmost part of the rainfall zone. The obvious mesoscale structure in the precipitation amounts is most likely related to the highly complex orography of the area. Between 0600 and 1200 UTC 13 November, the COL moves northeastward to central Nevada and weakens to 5601 gpm (Figs. 1e–f). During this period and the following 6 h, precipitation to the east and southeast of the COL center slowly weakens too.

Figure 2a shows the NARR precipitation accumulated over the 36-h time period covered in Fig. 1 (0600

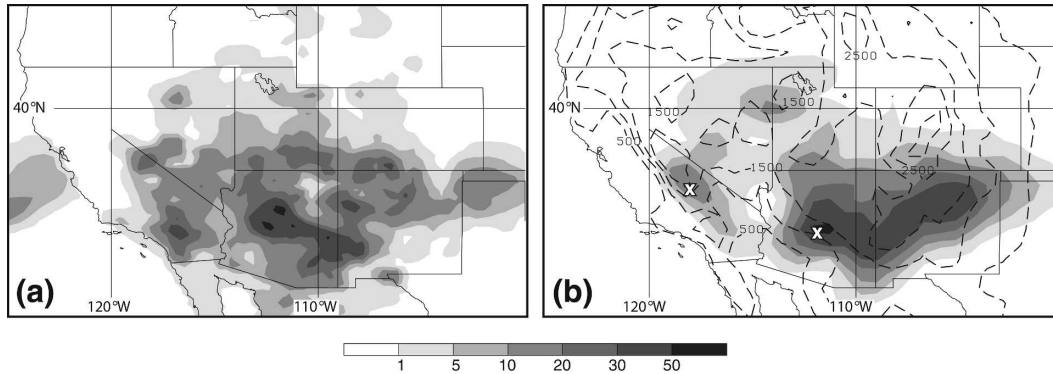


FIG. 2. The (a) 36-h (0600 UTC 12 Nov–1800 UTC 13 Nov 2003) accumulated precipitation (shading in mm) from the NARR. (b) As in (a) but for UW-NMS precipitation. The dashed isopleths depict the model orography (contoured every 500 m). The Xs mark the positions from where the trajectories in Figs. 6 and 7 were started.

UTC 12 November–1800 UTC 13 November). The area affected by the event stretches from the southern California coast to the panhandle of Texas and from northwestern Mexico to southern Idaho. The relatively low values to the south of the U.S.–Mexican border might in part be related to imperfect blending between the different gauge datasets used for NARR (Mesinger et al. 2006). Maximum gridpoint values of more than 50 mm are found in the San Bernardino Mountains in southern California and in the highlands of central Arizona. The most significant rainfalls, in a climatological sense, occur in the semiarid parts of southern California and Nevada (Mojave and Sonora Deserts). Table 1 contains the storm-total precipitation for selected stations in this region from the climatological data published by the National Climatic Data Center (NCDC). The highest storm total of 36 mm is observed at Lake Arrowhead in the San Bernardino Mountains, but several lower-elevation stations also record precipitation of more than 20 mm (Trona, Daggett, Twentynine Palms, and Palm Springs, California). Even at some very dry locations below sea level (Death Valley, Imperial, and Mecca Fire Station in California) precipitation of up to 13 mm is observed. Many stations at lower and intermediate elevation receive rainfalls on the order of 1–5 times the long-term November average and up to 24% of the mean annual sum, often over a period of only a few hours (not shown).

A comparison between storm totals from NARR and the precipitation simulated by the UW-NMS (Fig. 2b) reveals satisfactory agreement in both magnitude and spatial extent. The unusual precipitation in southern California and southern Nevada (Table 1), however, is not fully reproduced by the model. This (and the lack of fine structure in Fig. 2b) are most likely related to the smoothing of the extremely complex orography at the employed spatial resolution of 75 km (outlined by the

dashed lines in Fig. 2b), which implies weaker precipitation-enhancing effects like mechanical forcing for uplift, solar heating of steep slopes, katabatic acceleration of evaporationally cooled air, etc. The smoothed orography might also explain why the model displaces the maximum precipitation from the San Bernardino Mountains (below 1500 m in the model) toward the more elevated southern tip of the Sierra Nevada (more than 2000 m in the model). Nevertheless, the overall agreement appears sufficient to justify the use of the UW-NMS data for an analysis of the moisture transports and dynamics involved in this precipitation event.

#### 4. Synoptic evolution

Figure 3 displays the evolution of the low-level (left panels) and upper-level (right panels) circulation and thermal fields leading up to the precipitation event described in section 3. At 1200 UTC 10 November the dominating feature in the 1000-hPa geopotential height field is a pronounced subtropical anticyclone centered near 42°N, 149°W, which corresponds to a weak thermal ridge in the 900–500-hPa thickness field (Fig. 3a). Farther downstream is a distinct positively tilted trough, evident in both the low-level thickness and the jet-level (340 K) streamlines (Figs. 3a and 3b). The PV charts on the 325-K isentropic surface calculated from ECMWF TOGA data reveal that this trough results from the breaking of a large-scale PV wave over the North Pacific during 8–9 November and subsequent distinct stretching deformation similar to the idealized LC1 life cycle of baroclinic waves (Thorncroft et al. 1993; not shown). Along the equatorward flank of this trough lies a tight baroclinic zone that corresponds to a conspicuous 340-K jet with a maximum of  $64 \text{ m s}^{-1}$  over southeastern Utah (Figs. 3a and 3b). The jet entrance region is characterized by fairly widespread moderate

TABLE 1. Precipitation (mm) on 12 and 13 Nov 2003, and storm totals at selected stations in southern CA (station numbers starting with 7) and southern NV from NCDC climatological data. The last two columns show the respective percentages of the November and annual totals averaged over 1971–2000.

No.	Station name	County	Elev (m)	12	13	$\Sigma$	Nov (%)	Yr (%)
70822	Bishop AP	Inyo	1250	18	3	21	182	16
78406	South Lake	Inyo	2920	26	0	26	56	5
72319	Death Valley	Inyo	−59	0	11	11	375	19
73710	Haiwee	Inyo	1166	0	15	15	123	8
77253	Randsburg	Kern	1088	3	10	12	107	7
79035	Trona	San Bernadino	517	20	0	20	320	19
75890	Mountain Pass	San Bernadino	1442	1	22	23	138	10
73496	Goldstone Echo NO2	San Bernadino	899	8	16	24	396	17
70436	Baker	San Bernadino	287	15	0	15	246	16
72257	Daggett	San Bernadino	584	26	0	26	561	24
75721	Mitchell Caverns	San Bernadino	1326	2	14	17	114	6
76118	Nedless AP	San Bernadino	271	6	0	6	71	5
72771	El Mirage	San Bernadino	899	13	9	22	307	15
74671	Lake Arrowhead	San Bernadino	1586	36	0	36	41	3
79099	Twentynine Palms	San Bernadino	602	25	1	26	486	22
74297	Iron Mountain	San Bernadino	281	3	4	8	143	8
76635	Palm Springs	Rivers	130	28	0	28	379	21
72598	Eagle Mountain	Rivers	297	8	9	16	356	15
70927	Blythe AP	Rivers	120	8	0	8	174	8
75502	Mecca Fire Station	Rivers	−55	0	13	13	250	15
76386	Ocotillo Wells 2 W	San Diego	119	18	2	20	335	19
74223	Imperial	Imperial	−20	2	1	3	58	4
40718	Beatty 8 N	Nye	1082	17	6	23	224	15
45890	Pahrump	Nye	815	0	12	12	136	9
45880	Pahrnagat Wildlife Refuge	Lincoln	1036	0	14	14	106	8
42243	Desert National Wildlife Range	Clark	890	0	17	17	231	14
36691	Red Rock Canyon Spring	Clark	1152	0	21	21	111	8
44436	Las Vegas AP	Clark	648	12	0	12	158	11
47369	Searchlight	Clark	1079	0	12	12	100	6

cold advection at 700 hPa (shading in Fig. 3a) and by shallow cumulus clouds in IR imagery (Fig. 3b). A weak 1000-hPa inverted trough is found underneath the upper trough, but the circulation at this level is clearly dominated by northeasterly trade winds toward the geopotential height minimum along the ITCZ (dashed line in Fig. 3a), which is marked by cellular convection at about 9°N.

At 1200 UTC 11 November the low-level geopotential height field has not changed markedly, but the midlevel cold air has cut off near the California coast with some cellular convection to the south of the thickness minimum (Figs. 3c and 3d). A large region of cold advection and low-level cumuli is still found in the entrance region of the slightly intensified STJ. A conspicuous flare-up of ITCZ convection is evident in the IR image between 160° and 135°W. The 340-K streamlines indicate that outflow from this convection accelerates northeastward toward the localized regions of negative isentropic absolute vorticity (black lines in Fig. 3d). This situation is consistent with a modeling study by Blanchard et al. (1998) that shows how inertial in-

stability associated with regions of negative vorticity acts to intensify the divergent upper-level outflow from convection, particularly at low latitudes, where geostrophic adjustment is slow.

By 1200 UTC 12 November, when precipitation has just started in the region of midlevel warm advection over California and Arizona (Fig. 1a), the large subtropical anticyclone begins to weaken (Fig. 3e). Farther west, a surface cyclone forms ahead of an upper-level trough accompanied by strong midlevel cold advection and a distinct cloud band (Figs. 3e and 3f). The cold advection over the subtropical Pacific, in contrast, has weakened to the southwest of the inverted trough in the 1000-hPa geopotential height field. The secluded midlevel cold air approaches the California coast and even at 340 K a closed circulation is found in agreement with the 500-hPa geopotential height shown in Fig. 1b. The convective flare-up in the ITCZ has intensified and has spread northeastward toward the right entrance region of the upper jet, which still reaches a maximum of more than 60 m s<sup>−1</sup> close to San Diego (Fig. 3f). A contiguous elongated band of negative absolute vortic-

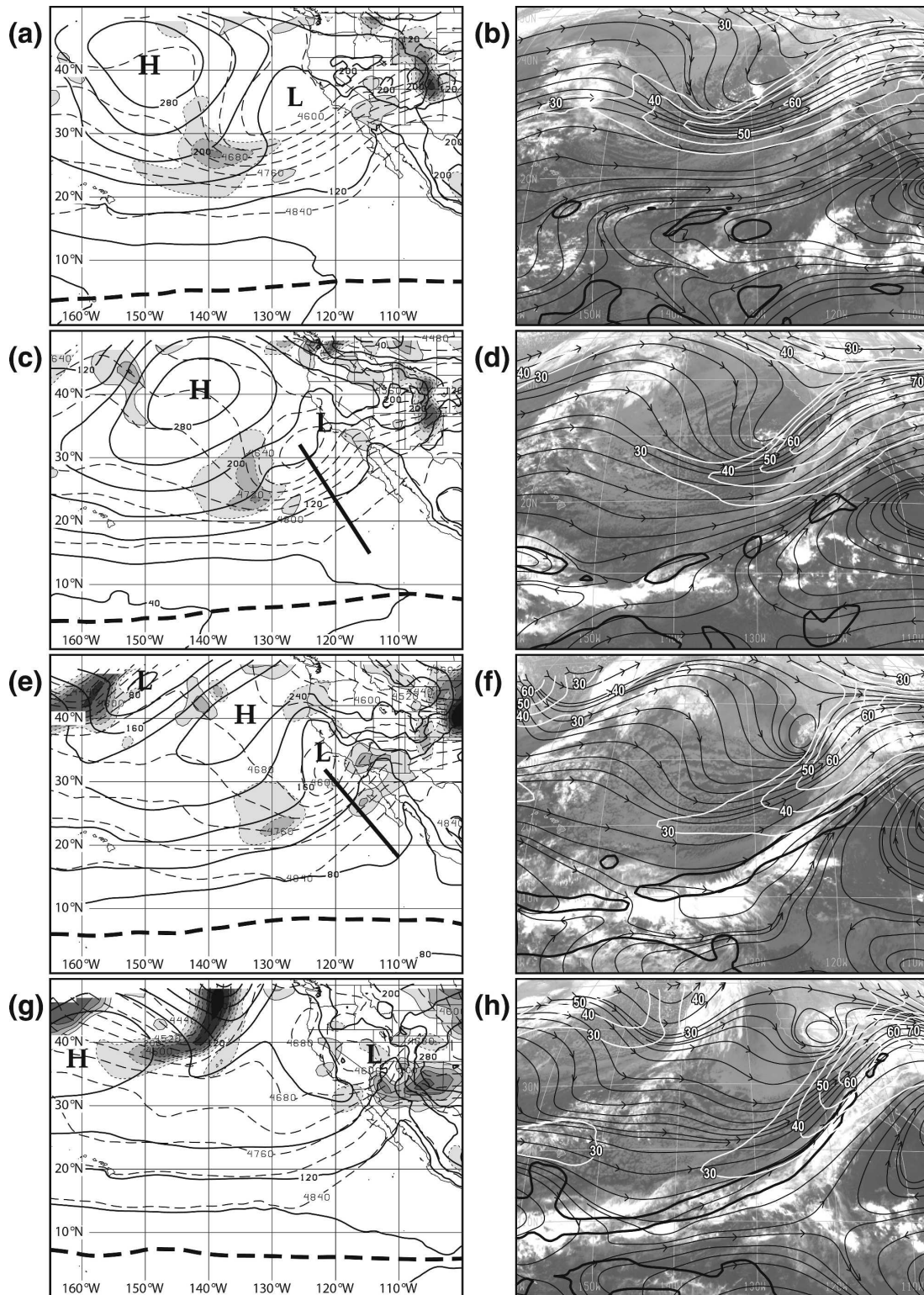


FIG. 3. (left) Geopotential height at 1000 hPa (solid isopleths every 40 gpm) with high and lows indicated, 900–500-hPa thickness (dashed isopleths every 40 gpm), and temperature advection at 700 hPa (shading; contours are  $\pm 5$ ,  $\pm 10$ ,  $\pm 15$ ,  $\pm 20$ ,  $\pm 30$ ,  $\pm 40 \times 10^{-5} \text{ K s}^{-1}$ ). The thick dashed lines mark the position of the equatorial pressure trough. (right) GOES IR satellite images with superimposed 340-K streamlines and isotachs (white isopleths every  $10 \text{ m s}^{-1}$  starting at  $30 \text{ m s}^{-1}$ ). The thick black contours border regions of negative absolute vorticity. The black lines in (c) and (d) indicate the positions of the cross sections in Figs. 8 and 10. Analysis times are 1200 UTC on (a), (b) 10, (c), (d) 11, (e) 12, and (f), (g) 13 Nov 2003.

ity stretches along the northern flank of the intensified ITCZ convection. Again this evolution is consistent with results of Blanchard et al. (1998) who show that convective outflow into a region of weak inertial stability can eventually create instability and thereby a positive feedback cycle that aids upscale growth. Farther north convective clouds wrap cyclonically around the COL center, giving it the appearance of an instant occlusion (cf. Fig. 21 in Browning 1986).

Finally at 1200 UTC 13 November, several hours after the greatest precipitation intensity (see Fig. 1), the COL has made landfall over California and Nevada (Figs. 1f, 3g, and 3h). The STJ on its equatorward side has reintensified to  $67 \text{ m s}^{-1}$  over Arizona (Fig. 3h). A continuous band of upper clouds stretches along the ITCZ and then northeastward across Baja California to the Colorado Rockies and into Texas. It clearly fulfills the definition of a TP formulated by McGuirk et al. (1987). The subtropical part of the TP is almost exactly parallel to the jet axis and is characterized by inertial instability along its poleward edge as far north as about  $35^\circ\text{N}$ . This evolution agrees with Mecikalski and Tripoli (1998) who suggest an important role for upper-level inertial instability in the formation of TPs. The precipitation over Arizona and New Mexico occurs in a region of moderate midlevel warm advection in association with the formation of a thermal ridge downstream of the COL (Fig. 3g). Some clouds reach across the jet axis and wrap around the COL center over Nevada, leading to the generation of the typical  $\lambda$  shape described in earlier studies (e.g., Thepenier and Cruette 1981). Some precipitation fell underneath this portion of the cloud band, too (Figs. 1e and 1f). To the immediate south and southeast of the COL center, an almost cloud-free region is evident in the IR image. This “dry slot” is typically found in connection with maturing intense extratropical cyclones. It should be pointed out that even at this stage, no distinct surface cyclone has formed underneath the COL (Fig. 3g).

A comparison between the UW-NMS fields just described and the ECMWF TOGA data reveals good overall agreement. The inverted trough at the surface is equally weak during 10–12 November, but at 1200 UTC 13 November the ECMWF data contain a slightly deeper low over Arizona. Geopotential heights in the ITCZ region are systematically a little higher in the ECMWF data. Good agreement is found between the STJs in the two datasets, but the absolute vorticity values along the anticyclonic side of the jet hardly reach negative values in the ECMWF data, which is at least, in part, related to the calculation of this quantity from finite differences and the coarser resolution of the latter dataset.

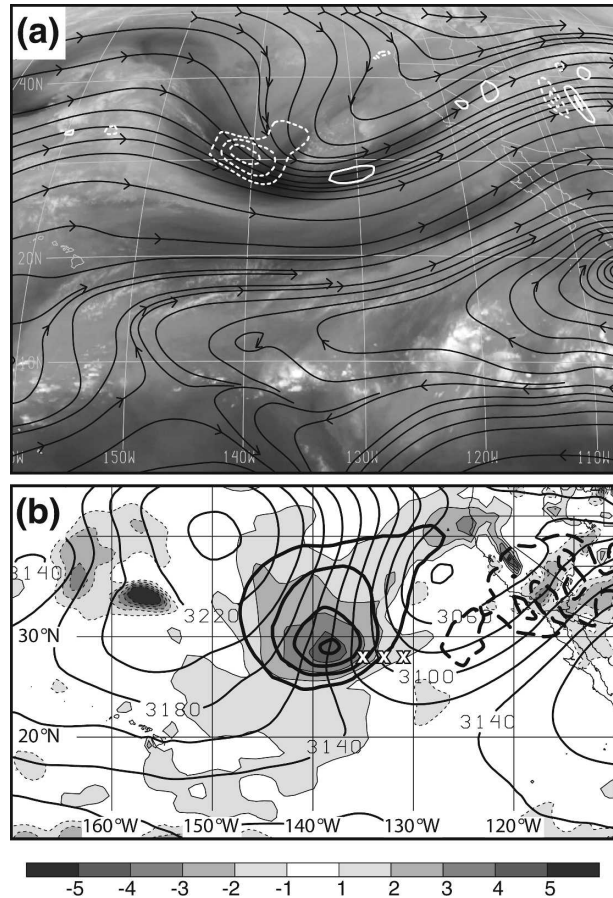


FIG. 4. (a) GOES WV satellite image with superimposed 340-K streamlines in black and divergence in white (every  $10 \times 10^{-6} \text{ s}^{-1}$ ). (b) Geopotential height (isopleths every 20 gpm),  $\omega_{OG}$  (thick isopleths every  $0.1 \text{ Pa s}^{-1}$ ), and model vertical velocity  $\omega$  (shading every  $0.1 \text{ Pa s}^{-1}$ ) at 700 hPa. Analysis time is 1200 UTC 10 Nov 2003. The Xs indicate the starting regions for the trajectories in Fig. 5.

## 5. The subsidence region

Part of the classical conveyor belt model for extratropical cyclones is the “dry airstream” that is related to the strong subsidence and drying behind the surface cold front (e.g., Carlson 1980; Browning 1990). Following up the discussion of the differences between the classical WCB and the low-latitude MCB in section 1, we will now address the subsidence region to the west of the COL described in section 4 and point out some differences as compared to the classical concept.

Figure 4a shows the 340-K streamlines from Fig. 3b and 340-K convergence superimposed onto the WV image of 1200 UTC 10 November. A zone of pronounced midlevel dryness is found around the base of the upper trough. It appears to be related to a conspicuous convergence maximum in the region of strong confluence

to the west of the upper trough and in the left entrance region of the STJ (Fig. 3b). For the same date, Fig. 4b shows geopotential heights and UW-NMS vertical motions  $\omega$  at 700 hPa. Strong subsidence of almost  $0.4 \text{ Pa s}^{-1}$  (about  $-5 \text{ cm s}^{-1}$ ) is found in the region of distinct zonal geopotential height gradients at 700 hPa, just to the southeast of the upper-level convergence maximum in Fig. 4a. To test if this subsidence is consistent with quasigeostrophic (QG) forcing, we solve the  $f$ -plane version of the QG omega equation with  $f_0$  set equal to  $30^\circ\text{N}$ , using the technique of successive overrelaxation. Input data are the model's gridded geopotential height and temperature fields after a bilinear interpolation to a  $1^\circ \times 1^\circ$  latitude–longitude grid at 12 isobaric levels (1000, 900, 800, 700, 600, 500, 400, 300, 250, 200, 150, and 100 hPa). The resulting QG vertical velocity  $\omega_{\text{QG}}$  (thick black lines in Fig. 4b) agrees with  $\omega$  in both structure and magnitude in the region of strongest subsidence. According to QG theory, subsidence can be forced by cold advection and/or an increase of negative vorticity advection with height. The former is clearly evident from Fig. 3a and the latter is most likely related to the  $\beta$  effect and the strong curvature in the northerly flow to the west of the trough axis (Fig. 4a).

As just explained, Fig. 4b suggests a mainly extratropical origin of the dry region. This is further corroborated by the fact that a narrow band of moister midlevel air separates it from the dry zone around  $20^\circ\text{N}$  that marks the subsiding branch of the Hadley circulation (Fig. 4a). The latter is characterized by weak, non-QG 700-hPa subsidence in the southeastern part of the subtropical anticyclone (Fig. 4b). The moist band appears to be fed by convection farther to the west, where ascent without considerable QG forcing is simulated by the model. To the east of the upper trough, where warm advection is evident in Fig. 3a, weakly negative  $\omega_{\text{QG}}$  is found. The model vertical motion, however, shows more concentrated ascent over California and Arizona, part of which is probably related to orographic effects. The same is most likely true for the simulated subsidence in central and northern California.

Figure 5 shows the evolution of three trajectories initiated in the subsidence zone at 700 hPa (white Xs in Fig. 4b). Figure 5a displays the trajectory tracks, and Figs. 5b–g show the evolutions of relative humidity (RH), water vapor mixing ratio (MR), height  $z$ , (equivalent) potential temperature  $\theta$  ( $\theta_e$ ), and the logarithm of total water condensate mixing ratio (LCMR). The latter was taken from the model's microphysics package as an indicator of clouds and precipitation. Between 7 and 9 November, trajectories 1 and 2 (T1 and T2; trajectories name T followed by the trajectory num-

ber hereafter) pass through a cyclonic circulation to the west of northern California/Oregon, accompanied by high RH and cloud formation. In contrast, T3 enters the domain with the cloud-free northerly flow to the west of the cyclone at 1200 UTC 8 November.

Around 0000 UTC 9 November all three trajectories reach the subsidence zone at about 6-km height. The westernmost T1 descends the most and sinks below 2 km early on 11 November with an MR (RH) of less than  $2 \text{ g kg}^{-1}$  (20%). Between 1200 UTC 11 November and 1200 UTC 12 November, the dry and adiabatically warmed air parcel passes through the PBL and surface fluxes from the ocean increase its water vapor content by about  $10 \text{ g kg}^{-1}$ , accompanied by large increases in RH and  $\theta_e$ . Assuming that this uptake is representative for the lowest kilometer ( $\sim 110 \text{ hPa}$ ) of the atmosphere would require an evaporation of more than  $11 \text{ mm day}^{-1}$ , about double the climatological value. This clearly demonstrates the increased energy transfer from the ocean necessary to bring this dry extratropical air mass closer to a thermodynamic equilibrium with the tropical ocean. Reaching  $10^\circ\text{N}$  on 13 November T1 becomes part of the ITCZ convection as indicated by the large increase in  $z$  ( $\sim 13 \text{ km}$ ) and  $\theta$  ( $\sim 50 \text{ K}$ ), decrease in MR ( $\sim 14 \text{ g kg}^{-1}$ ), and positive LCMR values. Interestingly,  $\theta_e$  continues to increase after LCMR becomes greater than zero at 0600 UTC 13 November. A potential reason for this is the additional latent heating from freezing processes at upper levels. Trajectory 2 shows a similar, but less dramatic, evolution with weaker subsidence and an involvement in less vigorous convection.

Despite the proximity to T1 and T2 during the first half of 10 November, T3 shows a very different evolution. It follows a cyclonic path into the southwestern United States, almost parallel to the dry zone evident in Fig. 4a. Subsiding substantially less than T1 and T2, T3 never enters the PBL, retains fairly low values of MR and RH and does not reveal strong changes in  $\theta$  or  $\theta_e$ . Around 0000 UTC 13 November, T3 passes the Los Angeles area at about 3-km height, close to the leading edge of the dry slot (Fig. 3f). Even though the UW-NMS is not capable of reproducing the extreme hailstorm over Los Angeles around this time (section 3), the path of T3 suggests an involvement in the production of potential instability via the differential advection of cooler dry air over moist warm air. The phenomenon of extreme convection at the leading edge of the dry slot has been documented in prior studies (e.g., Carr and Millard 1985; James and Clark 2003). A detailed analysis of this feature is beyond the scope of this paper.

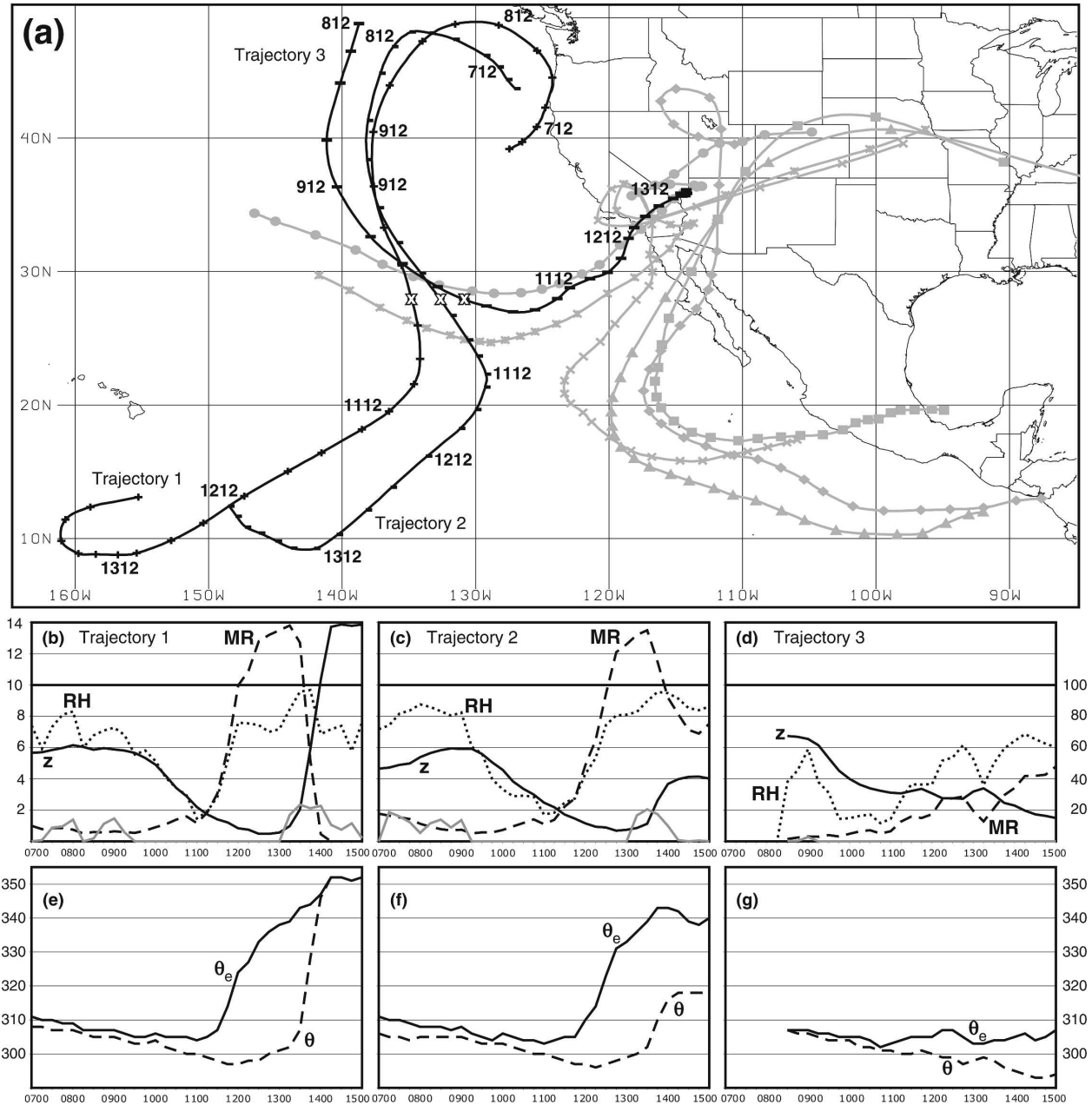


FIG. 5. (a) Trajectories started at 28°N and 135°, 133°, and 131°W (Xs) at 1200 UTC 10 Nov 2003 (black lines with markers every 6 h). The analysis times are indicated every 24 h. Gray lines and markers depict the trajectories from Figs. 6 and 7. (b)–(g) Quantities along trajectories: top panels show height  $z$  (solid; km),  $MR$  (dashed;  $g\ kg^{-1}$ ), LCMR (gray), and  $RH$  (dotted; %; ordinate on rhs.), while bottom panels show  $\theta_e$  (solid; K) and  $\theta$  (dashed; K).

The analysis of an ensemble of 561 trajectories initiated from the region 25°–30°N, 129°–133°W, and 750–650 hPa, reveals that the subjectively chosen trajectories T1–3 from Fig. 5 do in fact represent the major airstreams passing through the subsidence region (not shown). The most significant differences between these trajectories and the classical dry airstream are the relatively slow descent from midlevels [in contrast to upper

levels; see, e.g., Fig. 9 in Wernli (1997)] and the involvement of the subsided air in deep tropical convection after a substantial moistening through surface fluxes. The behavior of T1–3 shows similarities to an example documented by Wernli and Davies (1997, their Fig. 13) where upper-tropospheric air protrudes into the tropical PBL without a direct association with a surface cyclogenesis event.

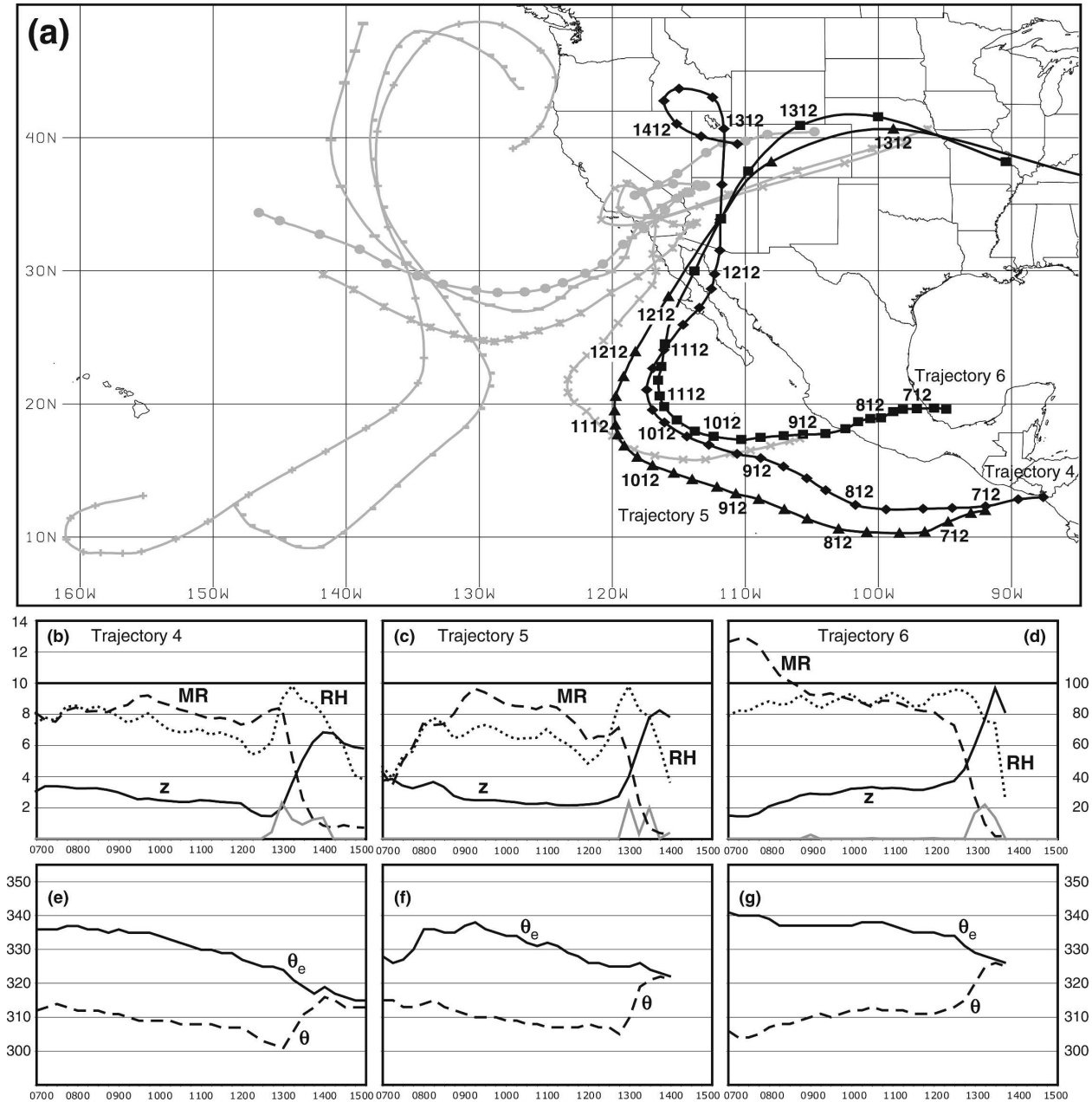


FIG. 6. As in Fig. 5 but for trajectories started in the precipitation region over AZ ( $34^{\circ}\text{N}$ ,  $112^{\circ}\text{W}$ ) at 0000 UTC 13 Nov 2003.

## 6. The MCB

This section provides a detailed analysis of the air masses involved in the formation of the MCB and the precipitation over the southwestern United States. As in section 5 we will assume both a Lagrangian (section 6a) and an Eulerian (section 6b) perspective.

### a. Lagrangian view

Two sets of three trajectories were started at different levels in the midtroposphere (2–6 km) at the time of

heaviest precipitation (0000 UTC 13 November; see Fig. 1): The first from the rainfall maximum over Arizona ( $34^{\circ}\text{N}$ ,  $112^{\circ}\text{W}$ ) and the second from the one over central California ( $36^{\circ}\text{N}$ ,  $118^{\circ}\text{W}$ ; see Fig. 2). The first set (T4–6) is characterized by an origin in the tropical lower troposphere (1.5–4 km) south of  $20^{\circ}\text{N}$  and an anticyclonic path into the precipitation region (Fig. 6). Trajectory 4 shows almost constant, high values of RH ( $\sim 70\%$ ) and MR ( $\sim 8 \text{ g kg}^{-1}$ ) during 7–12 November. The slight decrease in  $z$ ,  $\theta$ , and  $\theta_e$  during this period is presumably related to radiative cooling under the

cloud-free upper-level anticyclone (see Figs. 3b and 3d). During 0000–1800 UTC 12 November, subsidence, decreasing  $\theta$ , and an increase in RH and MR indicate evaporational cooling underneath the cloud band over northwestern Mexico. Between 1800 UTC 12 November and 0000 UTC 14 November, the trajectory circulates around the slowly northeastward-moving COL (Figs. 1c–f) and becomes part of the instant occlusion cloud feature (Fig. 3h) as shown by LCMR values greater than zero (Fig. 6b). Simultaneously, the parcel warms through latent heating, and drops most of its moisture content in the precipitation zone over Arizona and Utah while rising to almost 7 km.

The southernmost trajectory, T5, experiences a substantial moistening during 7–9 November, presumably caused by convective mixing in the ITCZ. Over the following days its evolution is almost identical to T4. Being a little closer to the midlevel wind maximum, it passes more quickly underneath the cloud band and shows less evidence for evaporational cooling. Getting lifted to over 8 km in the precipitation zone over Arizona, it follows the upper-level jet to the east instead of encircling the COL center as does T4. Finally, T6 originates in the very moist, low-level air over the Gulf of Mexico (MR of more than  $12 \text{ g kg}^{-1}$ ), and then warms and dries while rising over the mountains in central Mexico. After reaching the Pacific Ocean on 9 November its evolution closely follows T5, but evaporational cooling underneath the cloud band is weaker due to RH values of around 90%.

To corroborate the results shown in Fig. 6, we calculated an ensemble of 866 trajectories started from all model levels below 500 hPa in the region  $33^{\circ}$ – $35^{\circ}$ N,  $110^{\circ}$ – $114^{\circ}$ W at 0000 UTC 13 November. The analysis of this ensemble reveals that the majority of air parcels associated with WVFs of more than  $30 \text{ g kg}^{-1} \text{ m s}^{-1}$  originate from the midlevel (700–800 hPa) tropical easterlies with typical initial MR values of  $6$ – $12 \text{ g kg}^{-1}$  and then slowly circulate northeastward toward North America (not shown). Of all 194 trajectories fulfilling this criterion, only 43 originate from levels below 850 hPa (like T6) and most trajectories are quasi-horizontal before 0000 UTC 12 November. This is a very marked difference to the classical WCB and justifies the usage of the term MCB for this coherent trajectory ensemble. Trajectories ending below 800 hPa typically subside and moisten when approaching the precipitation region, most likely related to evaporational cooling (cf. T4), whereas trajectories above this level tend to rise and lose moisture.

Figure 7 depicts exemplary trajectories feeding the precipitation over California. Trajectory 7 (T7) behaves similarly to T4–6. During 7–8 November, T7 remains in

the low-level tropical easterlies with high MRs of  $10$ – $11 \text{ g kg}^{-1}$ . On 9 November, T7 curves anticyclonically and reaches the coast of Baja California around 1200 UTC 12 November. During this period MR and  $\theta_e$  markedly decrease. Between 0600 UTC 12 November and 0600 UTC 13 November, T7 starts circulating around the COL center over California (Figs. 1d and 1e), rises to 8 km, loses its moisture, and warms through latent heating. Subsequently the parcel sinks to almost 5 km and follows the midlevel easterly flow toward the central United States. The behavior of T7 and T4 is similar to, but at a higher elevation than, the polar trough conveyor belt discussed by Browning (1990, his Fig. 22). Figure 7a shows that T7 undercuts the dry trajectory T3 around 1800 UTC 12 November and thus contributes low-level moist, warm air to the convective destabilization over southeastern California (see section 5). In contrast, T8 and T9 have extratropical origins, track eastward around the base of the upper trough (see Fig. 1b), and reach North America around 0000 UTC 11 November. Both are part of the moist tongue seen in Fig. 4a. Being initially fairly dry, the MR along the southern T8 substantially increases between 9 and 12 November. After 1200 UTC 12 November, T8 behaves almost identically as T7 and contributes to the precipitation over California. Trajectory 9 experiences an initial moistening in a precipitation event over the Pacific Ocean on 7 November. Retaining high RH throughout the entire period 7–15 November, T9 does not actively contribute to the precipitation, but allows rain from higher levels to fall through it without substantial evaporation.

Again a trajectory ensemble was calculated for comparison; this time starting from  $35^{\circ}$ – $37^{\circ}$ N,  $120^{\circ}$ – $124^{\circ}$ W (not shown). In this ensemble only 27 trajectories (3.2%) fulfill the WVF criterion of  $30 \text{ g kg}^{-1} \text{ m s}^{-1}$ . Fourteen of these show a predominantly eastward track at midlevels with MRs of  $4$ – $6 \text{ g kg}^{-1}$  similar to T8 and T9. Nine trajectories originate at low or midlevels in the Tropics and initially show high MRs of more than  $10 \text{ g kg}^{-1}$  (cf. T7). In analogy to T7 and T8, the tropical trajectories tend to get drier, while at the same time the extratropical ones gain moisture. This points to a certain amount of mixing between the two airstreams, which could be partly related to trajectory calculation errors or numerical diffusion. Closer to North America evaporation of precipitation falling from the cloud band aloft is likely to contribute to the moistening, too (see the decrease in  $\theta$  along T8). In addition, the ensemble contains four trajectories with substantial WVFs that originate in the PBL at around  $50^{\circ}$ N and take cyclonic tracks into North America. These are not represented through an exemplary trajectory in Fig. 6. The results

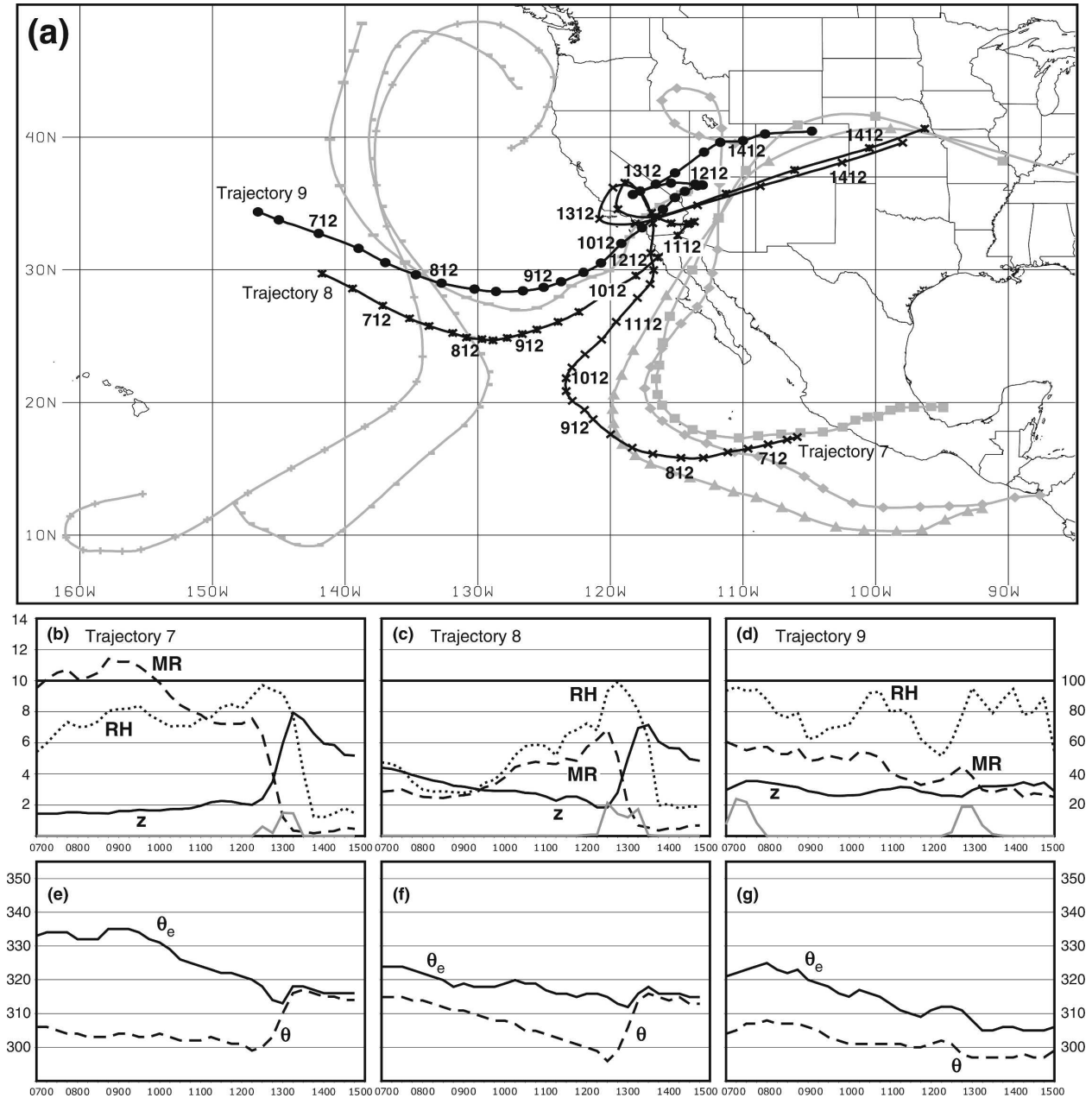


FIG. 7. As in Fig. 5 but for trajectories started in the precipitation region over CA ( $36^{\circ}\text{N}$ ,  $118^{\circ}\text{W}$ ) at 0000 UTC 13 Nov 2003.

suggest that T7 should clearly be regarded as part of the MCB, while T8 and T9 do not fulfill the MCB definition given in section 1 and might be considered an intermediate airstream. The region closer to the cyclone center is characterized by the convergence of moisture transports from various sources rather than a coherent MCB structure.

#### b. Eulerian view

We will now use horizontal and vertical cross sections through the MCB to analyze its structure from an Eu-

lerian perspective. For 1200 UTC 11 November, Fig. 8a shows 700-hPa geopotential heights, MR, and WVF, together with the positions of the trajectories from Figs. 5–7 at this time. South of about  $15^{\circ}\text{N}$ , easterlies dominate and MRs are around  $8 \text{ g kg}^{-1}$ . The MCB appears as a broad region of fairly high MR and large WVF that branches off from the tropical “reservoir” and stretches across Baja California toward northwestern Texas. The WVF maximum near  $26^{\circ}\text{N}$ ,  $116^{\circ}\text{W}$  is fed by tropical air as exemplified by T4–6, which are all close to the 700-hPa level at this time (Fig. 6). The

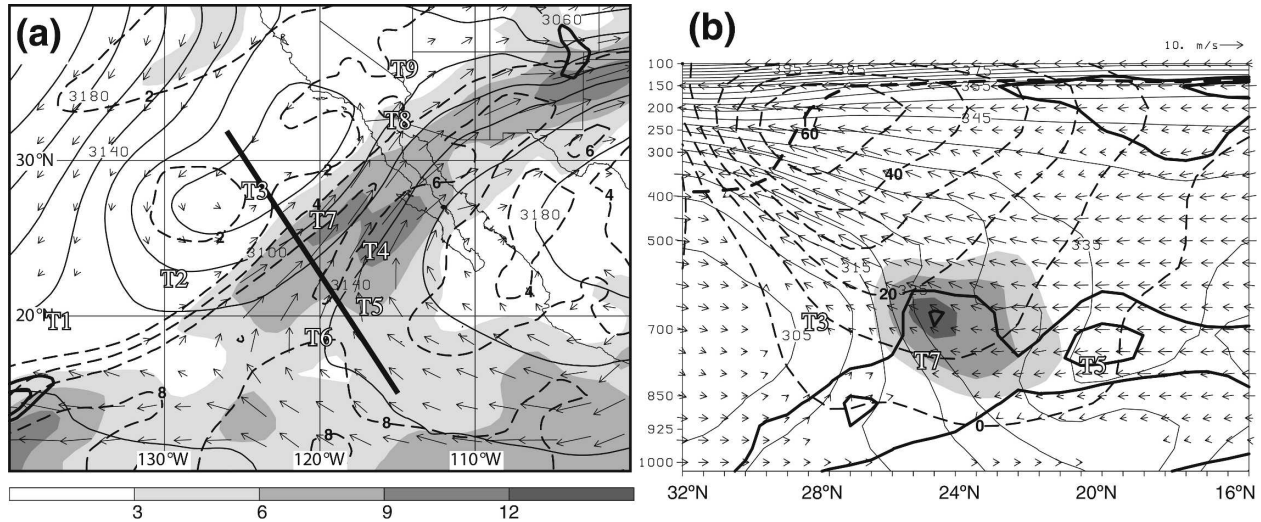


FIG. 8. (a) Geopotential height (solid isopleths every 20 gpm) and MR (dashed isopleths every 2 g kg<sup>-1</sup>) at 700 hPa for 1200 UTC 11 Nov 2003. Vectors and shading (according to legend; units are 10 g kg<sup>-1</sup> m s<sup>-1</sup>) depict 700-hPa WVF, thick black isopleths WVF convergence (every 5 × 10<sup>-5</sup> g kg<sup>-1</sup> s<sup>-1</sup> starting at 10 × 10<sup>-5</sup> g kg<sup>-1</sup> s<sup>-1</sup>). (b) Cross section along the black line shown in (a). Displayed quantities are circulation (vectors according to the scale in the top right corner with vectors smaller than 0.5 omitted; maximum ascent is 0.37 Pa s<sup>-1</sup>), θ<sub>e</sub> (thin solid lines every 5 K), wind speed (dashed lines every 10 m s<sup>-1</sup>) and WVF (shading every 20 g kg<sup>-1</sup> m s<sup>-1</sup> normal to cross section, PV (thick dashed line; 2 PV unit contour), RH (thick solid lines every 10% starting at 70%). The positions of the trajectories from Figs. 5–7 are marked.

second maximum farther west is associated with trajectories of tropical origin like T7. Both T8 and T9 have already reached the North American continent by this time and are located in the intermediate moist region wrapped around the center of the low-level cyclone. South of 30°N the poleward flank of the MCB is marked by a sharp MR gradient with values below 2 g kg<sup>-1</sup> on the dry side, where T1–3 are located. A somewhat moister region is found underneath the convection at the southern tip of the upper trough (Fig. 3d). No substantial WVF convergence is found along the MCB at this time. A comparison with ECMWF TOGA data shows satisfactory agreement in MR and WVF.

Figure 8b displays a cross section through the southern end of the MCB perpendicular to the low-level thermal wind (Fig. 3c). The upper trough is marked by a low dynamic tropopause as indicated by the 2-PVU contour (1 PVU = 10<sup>-6</sup> m<sup>2</sup> K<sup>-1</sup> s<sup>-1</sup>; thick dashed line in Fig. 8b). Wind speeds normal to the cross section reach 60 m s<sup>-1</sup> equatorward of this PV trough. The large vertical shear underneath the jet indicates a thermal front, but below about 700 hPa the shear weakens. Indications of a thermally direct cross-frontal circulation are evident. Near the surface, winds are predominantly northeasterly (i.e., out of the cross section). Relative humidity values greater than 70% characterize the region of moist tropical midlevel air (see the positions of T5 and T7). The MCB appears as a distinct maximum in WVF around 25°N and 700 hPa. While

horizontal gradients in θ only reach about 1.9 K 100 km<sup>-1</sup> at this level and even less below, the pronounced moisture decrease toward the dry extratropical air (see Fig. 8a) leads to large θ<sub>e</sub> gradients of 6.5 K 100 km<sup>-1</sup> poleward of the MCB with almost vertical moist isentropes. The weak surface thermal front and the high level of the WVF maximum both constitute substantial deviations from the WCB concept and back our new terminology. Close to the position of T5, even negative vertical gradients, and thus potential instability, are found. High RH values below the tropical tropopause at 16°–23°N reflect the beginning TP formation (Fig. 3d).

Figure 9 illustrates why poleward WVFs within MCBs maximize well above the PBL. The solid line shows geopotential height differences between the end points of the cross section from Fig. 8b (i.e., 15°N, 115°W and 32°N, 126°W). Below 800 hPa, these are negative due to the weak signature of the upper-level PV trough shown in Fig. 8b in the surface pressure field on one hand and the ITCZ pressure trough to the south on the other hand (see Figs. 3c and 3d), which results in a trade wind-like flow toward the Tropics. Above 800 hPa, height gradients increase and reach a maximum at the jet level (~200 hPa) between the upper low and the geopotential height maximum related to the outflow from tropical convection (not shown). The dashed line in Fig. 9 shows the MR profile at the tropical end of the cross section, where troposphere-deep easterlies pre-

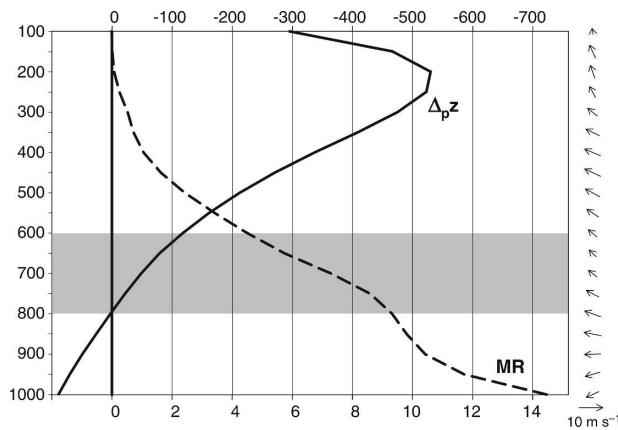


FIG. 9. Vertical profile at 15°N, 115°W at 1200 UTC 11 Nov 2003. Displayed quantities are total wind (vectors according to scale in bottom-right corner), MR ( $\text{g kg}^{-1}$ ; lower abscissa), and geopotential height difference to 32°N, 126°W (i.e., along the cross section in Fig. 8, gpm; upper abscissa). Values on the ordinate are in hPa.

vail (wind barbs). Above the PBL the moisture content in the tropical atmosphere decreases with height and halves between about 800 and 600 hPa (gray shading). In this layer both moisture and circulation conditions are favorable for a substantial moisture export to the extratropics. The implication for IWVFs is that large WVF values at midlevels will be partly compensated for by opposite contributions from the PBL that conceal the MCB transports.

At 1200 UTC 12 November, 1 day after the time shown in Figs. 8 and 9, the two 700-hPa WVF maxima have merged and intensified, and the MCB has narrowed under the influence of WVF convergence along its axis (Fig. 10a). While T4–6 are close to the core of the MCB, T7 and T8 are part of the less moist air that wraps around the intensified cyclone center (cf. Fig. 3f). Trajectory 3 is located near the leading edge of the dry slot. Considerable WVF convergence is also found in the convectively active region near 130°W (see Fig. 3f) and in the precipitation region between southern California and western New Mexico (see Fig. 1b), where WVF vectors indicate strong deformation in the region of the thermal ridge (cf. Fig. 3e). This situation is analogous to the rising of the classical WCB over the surface warm front, even though it occurs at a much higher level and is directly involved in the warm frontogenesis. WVFs within the MCB are somewhat smaller in the ECMWF data than in Fig. 10a with maxima differing by  $10 \text{ g kg}^{-1} \text{ m s}^{-1}$ . A cross section corresponding to Fig. 8b shows almost unchanged upper-level features and an MCB that has contracted to an intense maximum of high WVF and RH (Fig. 10b). The cold front is still confined to upper levels, while northeasterly winds

dominate near the surface (see Fig. 3e). Given the increased RH at the equatorward edge of the MCB, a release of the potential instability around 600 hPa is much more likely to occur than was the case 24 h earlier (cf. Fig. 8b).

Figure 11 shows 500-hPa geopotential heights, together with  $\omega_{\text{QG}}$  and model vertical velocity  $\omega$ , at the time of heaviest precipitation, 0000 UTC 13 November. The geopotential height minimum over the California coast is consistent between the UW-NMS, NARR, and ECMWF data within 13 gpm (cf. Fig. 1d). The uplift over California, Nevada, and Arizona is consistent with substantial QG forcing and is most likely enhanced through latent heat release. Over New Mexico, however, strong uplift is analyzed, where  $\omega_{\text{QG}}$  is rather small. Being fed by air from the equatorward part of the MCB, this ascent region is likely associated with a release of the aforementioned potential instability through orographic and weak large-scale forcing for uplift. Once established, convection benefits from weak inertial stability or even instability along the anticyclonic shear side of the STJ (see Fig. 3h) that facilitates the ventilation of upper-level outflow (e.g., Blanchard et al. 1998). This mechanism is presumably absent in most higher-latitude systems and points to a different precipitation distribution associated with MCBs in comparison with classical WCBs. As in Fig. 4b, the subsidence to the southwest of the upper cyclone is largely consistent with  $\omega_{\text{QG}}$ .

## 7. Discussion and conclusions

In this study we introduced a new terminology for bands of enhanced moisture transports at low latitudes and analyzed an example of the newly defined term MCB that occurred over the northeastern Pacific during 9–13 November 2003. MCBs are elongated bands of enhanced poleward WVFs above the PBL that are rooted in the Tropics. Phenomenologically they have to be distinguished from the classical midlatitude WCB (e.g., Carlson 1980; Browning 1990), TPs (McGuirk et al. 1987, 1988), and atmospheric rivers (Zhu and Newell 1994, 1998). The MCB under study was associated with significant precipitation in the semiarid southwestern United States including extreme hail in the Los Angeles area. The examination was based on satellite imagery, surface observations, ECMWF TOGA analyses, and output from a simulation performed using the UW-NMS, which reproduced the event with considerable fidelity, including the observed rainfall amounts. For the examination of the MCB we assumed both a Lagrangian and an Eulerian perspective. The following are the most important findings.

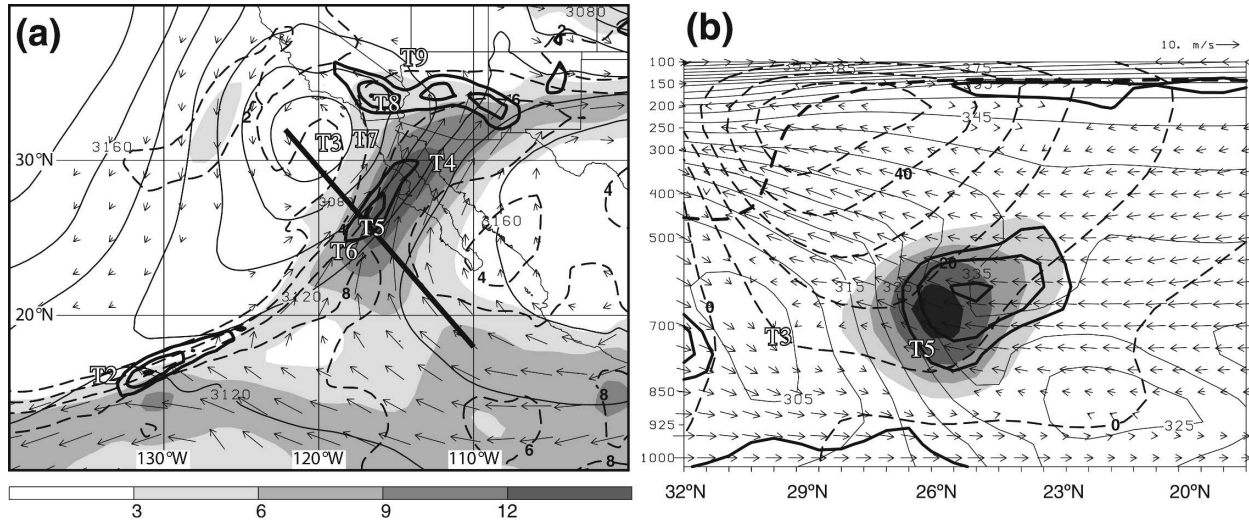


FIG. 10. As in Fig. 8 but for 1200 UTC 12 Nov 2003 (maximum ascent is  $0.28 \text{ Pa s}^{-1}$ ).

- The large-scale upper-level circulation is characterized by a wave-breaking event over the North Pacific that produces an almost stationary upper trough/COL off the California coast. The low-latitude location of the COL and its persistence are crucial factors, since they allow a prolonged tapping into moist tropical air. Surface cyclogenesis is weak.
- To the east of the trough is a strong STJ, associated with a pronounced upper-tropospheric baroclinic zone. At the surface, however, thermal contrasts are weak. At later stages a TP develops along the equatorward side of the STJ associated with a marked

flare-up of ITCZ convection and a strip of inertial instability as far north as  $35^\circ\text{N}$ .

- To the west of the trough there is a region of strong upper-level convergence, subsidence, cold advection, and drying, which produces a diffluent airstream with a cyclonic branch that feeds the dry slot to the south of the COL center and an anticyclonic branch that feeds the trade flow and eventually gets involved in ITCZ convection after large moisture uptakes from the ocean.
- The actual MCB consists of midlevel trajectories that curve anticyclonically away from the moist tropical easterlies. In the vicinity of the COL some trajectories curve around its center leading to the  $\lambda$ -shaped cloud feature typical for an instant occlusion. The flow along the upper-baroclinic zone leads to large northeastward WVFs, maximizing around 700 hPa. At lower levels northeasterly trade winds prevail. The moisture contrast between the MCB and the dry extratropical air farther north produces a strong  $\theta_e$  gradient in the lower troposphere.
- At late stages the frontogenetic circulation associated with the upper-jet leads to WVF convergence that involves airstreams from the midlevel subtropical and low-level midlatitude troposphere and narrows the MCB. This supports former criticism of the usage of the term atmospheric river, which does not reflect this aspect (Wernli 1997; Bao et al. 2006).
- The MCB-related precipitation occurs mainly to the east of the COL center, but also wraps cyclonically around it. Three regions can be distinguished. 1) Close to the COL center, moist low-level tropical air gets overrun by the leading edge of the dry slot, producing convective instability, the release of which ap-

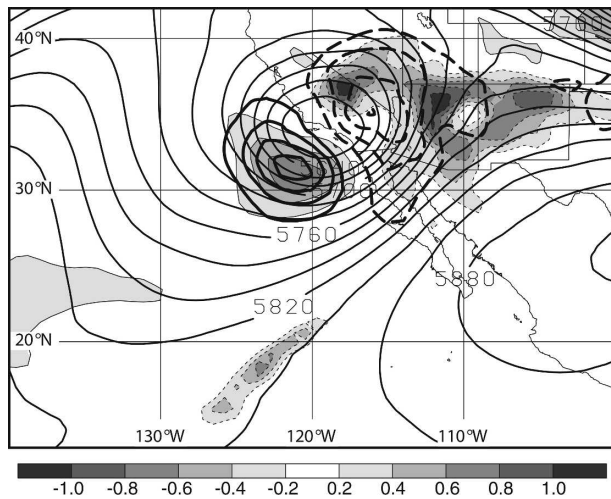


FIG. 11. Geopotential height (isopleths every 30 gpm),  $\omega_{OG}$  (thick isopleths every  $0.2 \text{ Pa s}^{-1}$  with negative values dashed), and model vertical velocity  $\omega$  (shading every  $0.2 \text{ Pa s}^{-1}$ ) at 500 hPa for 0000 UTC 13 Nov. 2003. The values of  $\omega_{OG}$  were calculated as in Fig. 4.

pears to have played a central role in the extreme hailstorm in the Los Angeles area. 2) To the north and east of the COL, strong QG forcing and midlevel warm frontogenesis generate ascent. Here, moist tropical air circulates around the COL and mixes with moderately moist (i.e., not strongly subsided) extratropical air. 3) Along the anticyclonic side of the STJ, very moist air at midlevels coincides with rather weak large-scale forcing. Here, precipitation generation benefits from the potential instability along the equatorward flank of the MCB and the inertial instability at the jet level. Most likely, orographic effects modify details of the precipitation distribution, but this effect has not been examined.

The most significant differences between the MCB and the classical extratropical WCB are the weak surface front and cyclone, the high elevation of maximum WVs, and the moist trajectories originating from above the PBL with slow, quasi-horizontal tracks associated with the MCB. These characteristics present some difficulties regarding its depiction on traditional weather charts. For instance, on hemispheric daily surface weather maps produced by the German Weather Service the upper-baroclinic zone to the north of the MCB discussed here is marked as a quasi-stationary surface cold front (not shown). This judgment is understandable given the scarce observations and the MCB's appearance on satellite imagery, but does not reflect its true characteristics.

A number of studies have demonstrated a relation between the neutral phase of the El Niño–Southern Oscillation (ENSO) and precipitation in the southwestern United States and adjacent Mexico (e.g., Higgins et al. 2000). During November 2003 the Climate Diagnostics Center multivariate ENSO index (information online at <http://www.cdc.noaa.gov/people/klaus.wolter/MEI/mei.html>) was small. A neutral-ENSO composite for extreme precipitation events in Tijuana, Mexico, reveals a number of similarities to the present case such as a positively tilted large upper wave over the North Pacific, a strong 200-hPa jet with maxima off California and over the central United States, as well as dry northerly flow west of 125°W and moist southerly flow to the east (Cavazos and Rivas 2004). According to Bao et al. (2006), the large-scale circulation during neutral ENSO years facilitates moisture transports from the Tropics over the eastern North Pacific. The present case is also consistent with the findings that ENSO warm phases suppress TP formation (McGuirk et al. 1987; Iskenderian 1995) and extratropical LC1 developments (Shapiro et al. 2001) in this region. The event examined here did, however, not occur during an active period of the

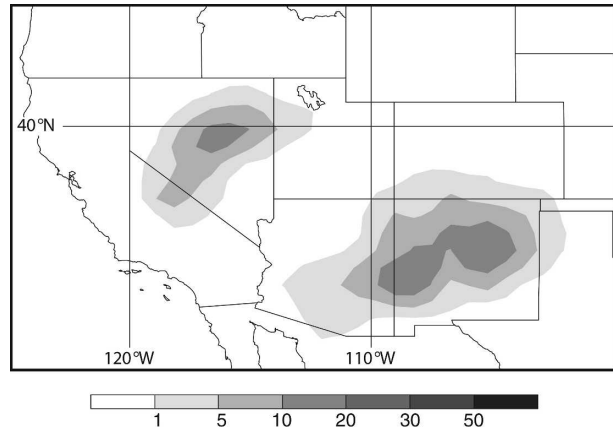


FIG. 12. Accumulated precipitation (mm; 0600 UTC 12 Nov–1800 UTC 13 Nov 2003) from a simulation with the UW-NMS initialized and updated with ECMWF instead of GFS data.

Madden–Julian oscillation (MJO) according to the Climate Prediction Center’s pentad MJO index (information online at [http://www.cpc.ncep.noaa.gov/products/precip/CWlink/daily\\_mjo\\_index/pentad.html](http://www.cpc.ncep.noaa.gov/products/precip/CWlink/daily_mjo_index/pentad.html)) in contrast to other cases of significant precipitation events in western North America.

A recently completed winter climatology of 330-K PV streamers and cutoffs identifies the North Pacific to the west of California as one of two occurrence maxima in the Northern Hemisphere with the other located off the coast of northwest Africa (Wernli and Sprenger 2007). For the latter region, Knippertz and Martin (2005) also find MCB-like moisture transports and TP formation during extreme cool season precipitation events in the northern Tropics and subtropics. During one of their cases a devastating localized thunderstorm occurred under the COL to the northwest of the TP (Fink and Knippertz 2003), similar to the hailstorm described in this paper.

It is noteworthy that a UW-NMS model run with the same resolution forced with ECMWF TOGA instead of GFS data was not able to adequately reproduce the rainfall event, despite the agreement in large-scale circulation features mentioned throughout the text. Accumulated precipitation amounts only reach maxima of 15 mm over central New Mexico and of 12 mm over central Nevada with a dry gap in between the two precipitation regions (Fig. 12), which quite dramatically deviates from Fig. 2b. A possible reason for this discrepancy is a more realistic midlevel MR field in the GFS data. For 1200 UTC 11 November, for example, 700-hPa GFS MRs are more than  $3 \text{ g kg}^{-1}$  higher in the tropical “root zone” of the MCB than in the ECMWF data (not shown). Generally, midlevel moisture fields can be expected to be of rather low quality over the Pacific

Ocean where direct observations are scarce and where the analysis relies on model forecasts and satellite data. As reported by Ralph et al. (2004), the analysis of lower-level WVs is exacerbated by problems with satellite retrievals in the presence of upper-level clouds and precipitation, for example, associated with a TP. The strong dependency of model results on the moisture field is corroborated by the fact that the Eta Model forecast initialized with GFS data successfully predicted the precipitation about 2 days in advance (not shown). Mesoscale modeling experiments with the fifth-generation Pennsylvania State University–National Center for Atmospheric Research Mesoscale Model and the Weather Research and Forecasting models using Eta Model output as initial and boundary conditions also show some ability to reproduce the unusual Los Angeles hailstorm (R. Fovell 2004, personal communication). More sensitivity studies are needed to unveil the effects of MCBs on precipitation over the southwestern United States and adjacent Mexico.

*Acknowledgments.* The scientific results presented in this paper were accomplished during the first author's two-year postdoctoral research scholarship from the German Science Foundation (DFG; Grant KN 581/1–2) at the Department of Atmospheric and Oceanic Sciences of the University of Wisconsin—Madison under the supervision of Prof. Jonathan E. Martin and Prof. (emeritus) Stefan L. Hastenrath. We wish to thank Pete Pokrandt and Greg Tripoli for assistance in running the UW-NMS model. We would like to acknowledge valuable comments from one anonymous reviewer and from Heini Wernli, who also introduced the first author to the Lagranto trajectory program.

## REFERENCES

- Bao, J.-W., S. A. Michelson, P. J. Nieman, F. M. Ralph, and J. M. Wilczak, 2006: Interpretation of enhanced integrated water vapor bands associated with extratropical cyclones: Their formation and connection to tropical moisture. *Mon. Wea. Rev.*, **134**, 1063–1080.
- Blanchard, D. O., W. R. Cotton, and J. M. Brown, 1998: Mesoscale circulation growth under conditions of weak inertial instability. *Mon. Wea. Rev.*, **126**, 118–140.
- Bond, N. A., and R. G. Fleagle, 1985: Structure of a cold front over the ocean. *Quart. J. Roy. Meteor. Soc.*, **111**, 739–759.
- Broder, J. M., and C. Dixon, 2003: Rain and hail deluge a slice of the Los Angeles basin. *New York Times*, 14 November 2003, late ed., A16.
- Browning, K. A., 1986: Conceptual models of precipitation systems. *Wea. Forecasting*, **1**, 23–41.
- , 1990: Organization of clouds and precipitation in extratropical cyclones. *Extratropical Cyclones: The Erik H. Palmén Memorial Volume*, C. Newton and E. Holopainen, Eds., Amer. Meteor. Soc., 129–153.
- Carlson, T. N., 1980: Airflow through midlatitude cyclones and the comma cloud pattern. *Mon. Wea. Rev.*, **108**, 1498–1509.
- Carr, F. H., and J. P. Millard, 1985: A composite study of comma clouds and their association with severe weather over the Great Plains. *Mon. Wea. Rev.*, **113**, 370–387.
- Cavazos, T., and D. Rivas, 2004: Variability of extreme precipitation events in Tijuana, Mexico. *Climate Res.*, **25**, 229–243.
- Eckhardt, S., A. Stohl, H. Wernli, P. James, C. Forster, and N. Spichtinger, 2004: A 15-year climatology of warm conveyor belts. *J. Climate*, **17**, 218–237.
- Fink, A. H., and P. Knippertz, 2003: An extreme precipitation event in southern Morocco in spring 2002 and some hydrological implications. *Weather*, **58**, 377–387.
- Hibbard, W., J. Anderson, I. Foster, B. Paul, R. Jacob, C. Schafer, and M. Tyree, 1996: Exploring coupled atmosphere-ocean models using Vis5D. *Int. J. Supercomp. Appl.*, **10**, 211–222.
- Higgins, R. W., J.-K. E. Schemm, W. Shi, and A. Leetma, 2000: Extreme precipitation events in the western United States related to tropical forcing. *J. Climate*, **13**, 793–820.
- Hoskins, B. J., M. E. McIntyre, and A. W. Robertson, 1985: On the use and significance of isentropic potential vorticity maps. *Quart. J. Roy. Meteor. Soc.*, **111**, 877–946.
- Iskenderian, H., 1995: A 10-year climatology of Northern Hemisphere tropical cloud plumes and their composite flow patterns. *J. Climate*, **8**, 1630–1637.
- James, R. P., and J. H. E. Clark, 2003: The diagnosis of vertical motion within dry intrusions. *Wea. Forecasting*, **18**, 825–835.
- Kiladis, G. N., 1998: Observations of Rossby waves linked to convection over the eastern tropical Pacific. *J. Atmos. Sci.*, **55**, 321–339.
- Knippertz, P., 2005: Tropical–extratropical interactions associated with an Atlantic tropical plume and subtropical jet streak. *Mon. Wea. Rev.*, **133**, 2759–2776.
- , and J. E. Martin, 2005: Tropical plumes and extreme precipitation in subtropical and tropical West Africa. *Quart. J. Roy. Meteor. Soc.*, **131**, 2337–2365.
- Kuhnel, I., 1989: Tropical–extratropical cloudband climatology based on satellite data. *Int. J. Climatol.*, **9**, 441–463.
- McGuirk, J. P., A. H. Thompson, and N. R. Smith, 1987: Moisture bursts over the tropical Pacific Ocean. *Mon. Wea. Rev.*, **115**, 787–798.
- , —, and J. R. Schaefer, 1988: An eastern Pacific tropical plume. *Mon. Wea. Rev.*, **116**, 2505–2521.
- Mecikalski, J. R., and G. J. Tripoli, 1998: Inertial available kinetic energy and the dynamics of tropical plume formation. *Mon. Wea. Rev.*, **126**, 2200–2216.
- , and —, 2003: Influence of upper-tropospheric inertial stability on the convective transport of momentum. *Quart. J. Roy. Meteor. Soc.*, **129**, 1537–1563.
- Mesinger, F., and Coauthors, 2006: North American Regional Reanalysis. *Bull. Amer. Meteor. Soc.*, **87**, 343–360.
- Ralph, F. M., P. J. Nieman, and G. A. Wick, 2004: Satellite and CALJET aircraft observations of atmospheric rivers over the eastern North Pacific Ocean during the winter of 1997/98. *Mon. Wea. Rev.*, **132**, 1721–1745.
- Shapiro, M. A., H. Wernli, N. A. Bond, and R. Langland, 2001: The influence of the 1997–99 El Niño–Southern Oscillation on extratropical baroclinic life cycles over the eastern North Pacific. *Quart. J. Roy. Meteor. Soc.*, **127**, 331–342.
- Thepenier, R.-M., and D. Cruette, 1981: Formation of cloud bands associated with the American subtropical jet stream

- and their interaction with midlatitude synoptic disturbances reaching Europe. *Mon. Wea. Rev.*, **109**, 2209–2220.
- Thorncroft, C. D., B. J. Hoskins, and M. E. McIntyre, 1993: Two paradigms of baroclinic-wave life-cycle behaviour. *Quart. J. Roy. Meteor. Soc.*, **119**, 17–55.
- Trenberth, K. E., 1992: Global analyses from ECMWF and atlas of 1000 to 10 mb circulation statistics. NCAR Tech Note NCAR/TN-373+STR, 191 pp. [NTIS PB92-218718/AS.]
- Tripoli, G. J., 1992: A nonhydrostatic numerical model designed to simulate scale interaction. *Mon. Wea. Rev.*, **120**, 1342–1359.
- Wernli, H., 1997: A Lagrangian-based analysis of extratropical cyclones. II: A detailed case study. *Quart. J. Roy. Meteor. Soc.*, **123**, 1677–1706.
- , and H. C. Davies, 1997: A Lagrangian-based analysis of extratropical cyclones. I: The method and some applications. *Quart. J. Roy. Meteor. Soc.*, **123**, 467–489.
- , and M. Sprenger, 2007: Identification and ERA-15 climatology of potential vorticity streamers and cutoffs near the extratropical tropopause. *J. Atmos. Sci.*, in press.
- Zhu, Y., and R. E. Newell, 1994: Atmospheric rivers and bombs. *Geophys. Res. Lett.*, **21**, 1999–2002.
- , and —, 1998: A proposed algorithm for moisture fluxes from atmospheric rivers. *Mon. Wea. Rev.*, **126**, 725–735.